Structural and photoluminescence properties of Gd implanted ZnO single crystals

P. P. Murmu,[1,2,3] R. J. Mendelsberg,[3,4] J. Kennedy,[1,3,a)] D. A. Carder,[1,3] B. J. Ruck,[2,3] A. Markwitz,[1,3] R. J. Reeves,[3,4] P. Malar,[5] and T. Osipowicz[5]
[1]*National Isotope Centre, GNS Science, P.O. Box 31312, Lower Hutt, New Zealand*
[2]*School of Chemical and Physical Sciences, Victoria University of Wellington, P.O. Box 600, Wellington, New Zealand*
[3]*The MacDiarmid Institute for Advanced Materials and Nanotechnology, New Zealand*
[4]*Department of Physics and Astronomy, University of Canterbury, P.O. Box 4800, New Zealand*
[5]*Centre for Ion Beam Applications, Department of Physics, National University of Singapore, 117542, Singapore*

(Received 4 April 2011; accepted 24 June 2011; published online 12 August 2011)

We present the structural and photoluminescence properties of 30 keV gadolinium implanted and subsequently annealed zinc oxide (ZnO) single crystals. Rutherford backscattering and channeling results reveal a low surface region defect density which was reduced further upon annealing. For low implantation fluence, around 85% of the Gd atoms are estimated to be in sites aligned with the ZnO lattice, while for higher fluences the Gd is largely disordered and likely forms precipitates. The Raman spectra of the implanted samples show defect-induced modes, which match the one-phonon density of states for the most heavily implanted samples. Annealing eliminates these features implying the removal of Gd-associated lattice disorder. Low temperature photoluminescence spectra revealed a red-shift in the defect emission, from green to orange/yellow, indicating the suppression of a deep level, which is thought to be due to oxygen vacancies. It is suggested that the orange/yellow emission is unmasked when the green emission is quenched by the presence of the implanted Gd atoms. © *2011 American Institute of Physics*. [doi:10.1063/1.3619852]

I. INTRODUCTION

Zinc oxide (ZnO) has many useful properties, giving it the potential to be used for advanced optoelectronic and spintronic applications.[1] It shows rich UV emission due to free excitons and neutral donor bound excitons.[2] A variety of deep level emissions in the visible spectrum are also observed that are commonly assigned to intrinsic defects such as oxygen vacancies (V_o), zinc interstitials (Zn_i), and antisite disorder (O_{Zn}). However, the exact nature and source of the visible band emission remains elusive. For example, various green emissions have been attributed to transitions related to oxygen vacancies (V_o),[3] zinc interstitials (Zn_i),[4] antisite disorder (O_{Zn}),[5] or Cu impurities.[6] However, most studies suggest V_o as the dominant mechanism for the green emission, but several centers with overlapping emissions likely exist simultaneously in many samples. Additionally, there is uncertainty in the charge states of V_o and location in the bandgap of ZnO.[7]

Transition metals (TM) or rare-earth (RE) ions are often intentionally doped into ZnO in an attempt to form a dilute magnetic semiconductor. There are several reports of room temperature ferromagnetism in ZnO-based dilute magnetic semiconductors, including ZnO:TM (TM = Sc-Zn),[8] ZnO:Gd,[9,10] and ZnO:Er.[11] Notably, though, ferromagnetism has even been reported in undoped but defective ZnO,[12] making an interpretation of the role of the dopant ions uncertain. Theoretical predictions of the T_c value also critically depend upon the exact details of the incorporation of the dopant ions and the defect structure.[8] Thus, careful experimental investigation is essential to determine the bonding configuration around the dopant ions, and to identify the presence of any magnetic secondary phases.

Rare earth (RE) ions are very interesting dopant elements for optoelectronics and spintronic applications, due to their intra *f*-shell transitions and high orbital angular momentum. Several reports on RE element (e.g., Eu, Er, Tm, and Tb) doped GaN and ZnO have investigated the dopant locations, as well as the luminescence and magnetic properties.[13–17] Rare earth related optical centers have been observed in GaN and ZnO, and their spectral transitions range from the UV/blue to near infrared.[13–16] Usually, RE elements (e.g., Tm and Er) occupy the substitutional lattice sites, and require high defect densities for optical activation.[13] The suppression of some deep level optically active defects and the appearance of new defects can be observed due to implantation and annealing in RE- doped ZnO single crystals.[13] Monteiro *et al*. observed an enhanced broad violet band around 3.15 eV in Tm implanted and annealed ZnO which they assign to the zinc vacancy (V_{Zn}) related emission. In addition, Gd^{3+} is reported to have a radiative transition centered at around 318 nm between the first excited state $^6P_{7/2}$ and the ground state $^8S_{7/2}$, as shown in cathodoluminescence spectra in Gd-doped GaN.[17] A transition at 652 nm was also reported in Gd-doped GaN, which originates from the Gd^{2+} state.[17] Ney *et al*. reported a broad red emission in Gd implanted ZnO single crystals, which is attributed

a)Author to whom correspondence should be addressed. Electronic mail: j.kennedy@gns.cri.nz.

to implantation induced disorder rather than Gd related transitions.[10] Gadolinium has also been shown to be a suitable dopant for possible spintronic applications in GaN.[18] Previously reported investigations for Gd-doped ZnO have been mainly focused in terms of the spintronic aspects,[9,10] with relatively few reports on the optical properties. In this study we present the effects of Gd inclusion at various concentrations into ZnO, and the subsequent effects on the structural and photoluminescence properties.

II. EXPERIMENTAL PROCEDURE

The O-polar face of hydrothermally grown ZnO (0001) single crystals (Tokyo-Denpa) were implanted with 30 keV Gd ions under normal incidence. The samples were implanted at ambient temperature in a high vacuum chamber (on the order of 1×10^{-7} mbar) at the GNS Science low-energy ion implanter facility.[19] Gadolinium implantation fluences ranged from 4.6×10^{14} to 1.2×10^{16} ions cm^{-2} resulting in simulated Gd concentrations of 0.5 to 8.9 at. % below the surface region. The DYNAMIC-TRIM[20] calculations show an average implantation depth of $R_P \sim 10$ nm with a maximum depth of ~20 nm. The implanted samples were subsequently annealed in vacuum (base pressure $\sim 1 \times 10^{-7}$ mbar) at 750 °C for 30 min. Rutherford backscattering spectrometry (RBS) measurements were performed, using a 2 MeV He^+ beam, for compositional analysis and depth profiling of the implanted region. The crystalline quality of the implanted and subsequently annealed ZnO was analyzed, using the RBS channeling (RBS/C) technique,[21] where the incident beam was aligned along ZnO [0001]. Structural characterization was carried out by Raman spectroscopy measurements using a Jobin-Yvon LabRam micro-Raman system at room temperature. An Ar^+ laser at 514 nm was used as the excitation source with the Raman spectra collected utilizing a liquid nitrogen cooled CCD detector in backscattering geometry. Temperature dependent photoluminescence (PL) measurements were performed using a He-Cd laser (325 nm) with the samples placed in a liquid-He cooled cryostat with an integrated heating element, as described elsewhere.[22]

III. RESULTS AND DISCUSSION

The incorporation of the implanted Gd into the ZnO matrix and the resulting lattice disorder was investigated using Rutherford backscattering spectrometry. Standard (random) RBS measurements were performed to determine the retained dose (the fraction of implanted Gd that remains in the lattice). It was found that for fluences up to 1×10^{15} ions cm^{-2} all of the Gd atoms are retained in the ZnO, as indicated in Table I. However at higher fluences, up to 17% of the implanted ions are subsequently sputtered out, as expected after low energy and high fluence implantation.

We have used the RBS channeling (RBS/C) technique to study the crystalline quality and the location of dopant atoms incorporated into the lattice. The channeling minimum yield (χ_{min}) indicates the overall level of crystalline defects in the lattice, and is defined as the ratio of backscattered yield from a given atomic species when the incident beam is aligned to a crystallographic axis to that for a random beam incidence.[21] Therefore, an amorphous material shows a χ_{min} of 100%, whereas a perfectly single crystal may have a χ_{min} as low as ~1–2%. It should be noted that a significant channeling effect is expected not only from substitutionally implanted atoms, but also from atoms in any interstitial site that lies in line with a column of atoms in the crystal that is aligned with the incident RBS beam (the "shadowing effect").

In Fig. 1(a) the RBS spectra of as-received ZnO and ZnO implanted with a fluence of 9.0×10^{14} ions cm^{-2} both before and after annealing are shown. The RBS/C of as-received ZnO along the [0001] axis shows $^{Zn}\chi_{min}$ of ~4%, which is indicative of the good crystalline quality of the ZnO templates. The $^{Zn}\chi_{min}$ value for 9.0×10^{14} ions cm^{-2} implanted ZnO is around 18%, decreasing to 9% upon vacuum annealing at 750 °C. The low value of χ_{min} after implantation suggests that only a relatively low level of structural defects are introduced due to the Gd ion implantation, and there is a further recovery of the crystalline quality upon annealing. Substantially larger values for $^{Zn}\chi_{min}$ of 42 and 53% have been reported for 0.6 and 1.5% Gd implanted ZnO single crystals.[9] The lower Gd fluences used in this study have similar Gd concentrations retained in a shallower region of the sample, resulting in a lower level of structural defect formation upon implantation.

Figure 1(b) shows angle-dependent RBS scans performed along [0001] for 4.6×10^{14}, 9.0×10^{14}, and 1.2×10^{16} ions cm^{-2} implanted and annealed ZnO. The proportion of Gd atoms at either substitutional Zn sites (Gd_{Zn}) or shadowed interstitial sites along the ZnO *c*-axis can be

TABLE I. Fluence, retained dose, half-angles, and χ_{min} for unannealed and annealed Gd-implanted ZnO.

Fluence	Retained dose	Annealing	Half angles ($^{Zn}\chi_{1/2}$)(°)	$^{Zn}\chi_{min}$(%)	Half angles ($^{Gd}\chi_{1/2}$)(°)	$^{Gd}\chi_{min}$(%)
(Gd cm^{-2})	(Gd cm^{-2})					
As received	…	…	…	4	…	…
4.6×10^{14}	4.6×10^{14}	Unannealed	0.58	16	0.60	16
4.6×10^{14}	4.6×10^{14}	750°C	0.54	9	0.58	22
9.0×10^{14}	9.0×10^{14}	Unannealed	0.58	18	0.60	18
9.0×10^{14}	9.0×10^{14}	750°C	0.56	9	0.56	40
1.2×10^{16}	1.0×10^{16}	Unannealed	0.62	66	0.63	87
1.2×10^{16}	1.0×10^{16}	750°C	0.61	22	0.57	92

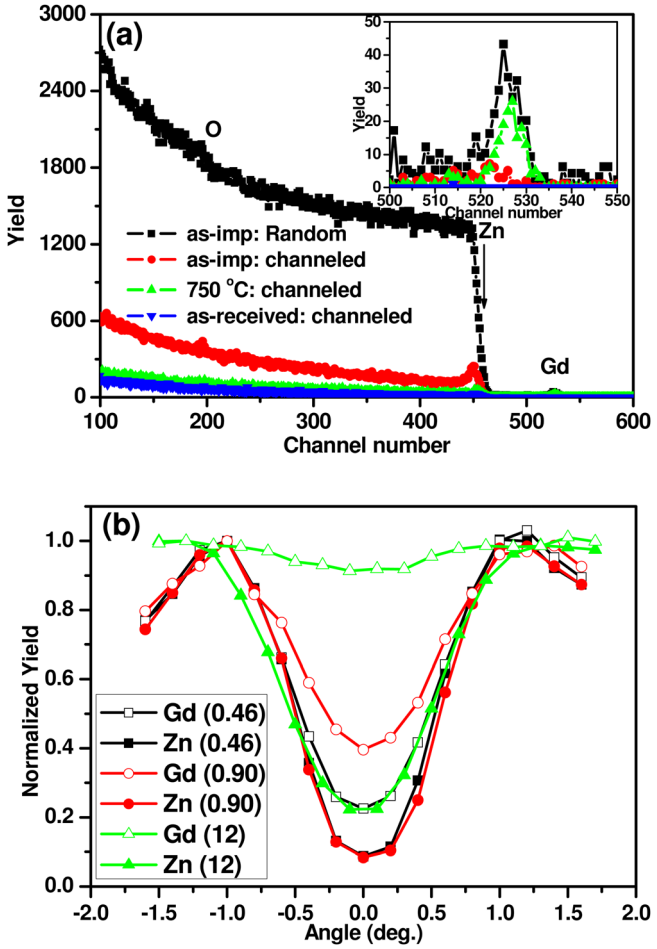

FIG. 1. (Color online) (a) Random and [0001]-aligned RBS spectra of 9.0×10^{14} ions cm^{-2} implanted and annealed ZnO. Inset shows the magnified Gd peaks. (b) Angular scans along the [0001] direction measured for 4.6×10^{14}, 9.0×10^{14}, and 1.2×10^{16} ions cm^{-2} implanted and annealed ZnO. Fluences are shown in the brackets with a unit of 10^{15} ions cm^{-2}.

estimated from χ_{min} for Gd and Zn using the formula $(1 - {}^{Gd}\chi_{min})/(1 - {}^{Zn}\chi_{min})$.[21] The angular scans for Gd and Zn almost overlap for the low fluence as-implanted ZnO (not shown) with small values for χ_{min}, which indicates that the Gd and Zn are subjected to similar low levels of disorder. The measured ${}^{Zn}\chi_{min}$ and ${}^{Gd}\chi_{min}$ for the lower fluence implanted and annealed ZnO samples are around 9 and 22–40%, respectively (see Table I). This suggests that 65–85% of the Gd atoms are at well defined sites along the ZnO *c*-axis contributing to the channeling effect, with the remaining atoms in sites not aligned with the ZnO *c*-axis. For a higher Gd fluence (1.2×10^{16} ions cm^{-2}) only around 11% of the Gd atoms are at ordered sites following annealing.

The half–angle ($\psi_{1/2}$) of the channeling dip, defined as the angle at which the normalized yield from the host atoms attains half of the value between the channeled and random yield,[21] can be used to further investigate the Gd atom incorporation. The Zn and Gd half-angles in as-implanted samples are very similar, implying that most of the Gd atoms are located in Zn substitutional sites and/or columns aligned along [0001], which is consistent with the aforementioned conclusions. Only a slight diminution in Zn and Gd half-angles is observed upon annealing compared to the as-implanted samples. However, a distinct difference between Zn and Gd half-angles in 4.6×10^{14} and 1.2×10^{16} ions cm^{-2} implanted and annealed samples suggests that some of the Gd atoms are slightly displaced from the Zn substitutional sites and/or shadowed columns.

These results indicate that for low fluences the as-implanted samples have most of the Gd atoms incorporated in sites that align with the ZnO lattice (either substitutional or shadowed), although there is some disorder associated with both species since ${}^{Zn}\chi_{min}$ decreases after annealing. On the contrary, for high implantation fluences, or for any of the annealed samples, the Gd ions exhibit a much higher level of disorder than the Zn ions. We interpret this as evidence of the formation of Gd clusters in the ZnO lattice after high-fluence implantation or after annealing of the implanted samples at 750 °C. Only the low fluence unannealed samples exhibit substantial incorporation of the Gd ions into the ZnO lattice. It is interesting to compare this behavior to the results from other implantation studies, where it has been reported that Tm and Er in ZnO predominantly occupy substitutional lattice sites, whereas Eu and Tb do not follow a similar trend.[13]

The structural properties of the samples were further investigated using Raman spectroscopy. Figure 2 shows the Raman spectra of ZnO implanted with Gd fluences between 4.6×10^{14} and 1.2×10^{16} ions cm^{-2}, along with spectra from an as-received and a 4.6×10^{14} ions cm^{-2} implanted and 750 °C annealed sample. The spectrum of the as-received sample is dominated by the strong E_2(low) and E_2(high) Raman peaks at 100 and 438 cm^{-1}, respectively. Weaker features at 205 and 332 cm^{-1} are assigned to the second order structure of $2E_2$(low) and $2E_2$(M).[23] A small peak at 575 cm^{-1} can be attributed to the A_1(LO) mode of ZnO, which becomes Raman active in the presence of disorder.[24,25]

The intensity of the $2E_2$(low) and $2E_2$(M) peaks decreases as the implantation fluence increases, which is consistent with increasing levels of implantation-induced disorder. At the same time, a broad background extending to low wavenumber appears with an intensity that increases

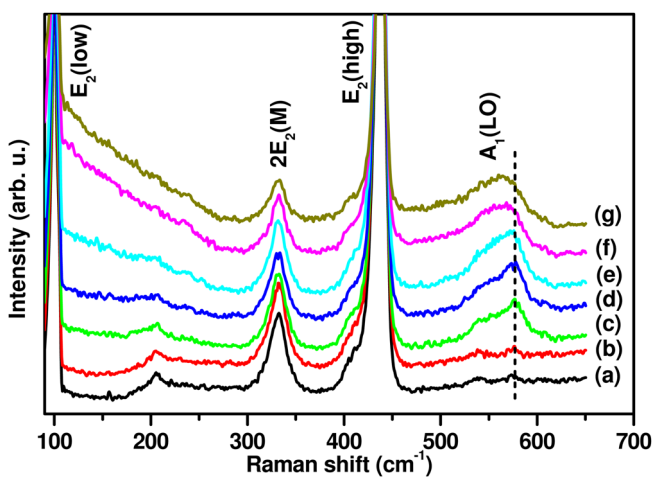

FIG. 2. (Color online) Raman spectra of (a) as-received, (b) 4.6×10^{14} (750 °C), (c) 4.6×10^{14}, (d) 9.0×10^{14}, (e) 2.9×10^{15}, (f) 7.2×10^{15}, and (g) 1.2×10^{16} ions cm^{-2} implanted ZnO (spectra vertically offset for clarity).

with implantation fluence. Because of the ion-implantation, the ZnO lattice is disordered which leads to the loss of translational periodicity, and hence the relaxation of $\mathbf{q} = 0$ conservation. This leads to scattering from the entire Brillouin zone, and so the broad background in the region from 100 to 200 cm^{-1} is similar to the one-phonon density of states (DOS).[28] This feature is enhanced in the high fluence implanted samples due to the increased level of disorder.

Most strikingly, substantial changes are observed in the region near the A_1(LO) peak at 575 cm^{-1}. For moderate implantation fluence the A_1(LO) peak increases dramatically in intensity, accompanied by a shoulder extending down to about 520 cm^{-1}. As the implantation fluence increases, the features in this region broaden and the peak shifts downward in energy. After annealing we observe an almost complete removal of the scattering between 500 and 600 cm^{-1} [see Fig. 2, curve (b)] such that it again resembles the unimplanted ZnO.

The broad feature from 520–575 cm^{-1} has been reported in ZnO implanted with various ions (e.g., H, N, P, and Mn).[24–27] In the case of P implanted ZnO, Chen *et al*. have attributed this scattering to the activation of silent Raman modes by disorder,[25] most notably, V_o. The Gd implantation induces considerable disorder in the ZnO, including V_o, so a similar interpretation could be applied to our data. The width of the feature matches that of the ZnO upper optical phonon branch, indicating that the entire branch becomes Raman active, and in fact, for the most heavily implanted samples the feature matches well with the shape of the calculated one-phonon (DOS) in this energy range.[28] Similar behavior has been observed in Mn implanted ZnO, and also assigned mainly to the activation of Raman modes by V_o.[24] However, we note that for the moderately implanted samples the feature displays a peak near 575 cm^{-1}, which matches the location of the calculated zone center A_1(LO) mode rather than the peak in the one-phonon DOS. This is suggestive of the interpretation of Friedrich *et al*. who ascribed the scattering to a resonant Raman process involving disorder-induced bound excitons that provide electronic states in the ZnO bandgap, which allow resonance at excitation energies below the gap.[26] The 514 nm excitation wavelength used here is similar to the 458 nm wavelength used by Friedrich *et al*. It seems likely that both effects can play a role in our samples, with the resonant process most prominent at lower implantation fluence. In any case, the scattering is clearly associated with lattice disorder associated with the implantation, and the disappearance of this scattering after annealing matches our conclusions from RBS measurements that annealing leads to precipitation of the Gd out of the ZnO matrix.

Low temperature (4 K) photoluminescence was observed from the O-polar face of the ZnO crystals before and after implantation and/or annealing, as shown in Fig. 3(a). As-received wafers show strong UV emission from neutral donor bound *A*-excitons I_4, I_5, and I_6, which have been attributed to hydrogen, unknown, and aluminum donors, respectively.[2] A broad band is seen in the region where *B*-excitons bound to the same neutral donors are expected (I_x^B). Ionized donor bound *A*-excitons emit at higher energies, denoted as I_x^+, which die out quickly with increasing temperature. Free exciton emission can also be observed from the longitudinal and transverse *A*-excitons (A_T and A_L), with a weak shoulder where the transverse B_T exciton is expected.[29]

Annealing the as-received wafer in vacuum at 750 °C for 30 min sharpens the emission but reduces the overall intensity; in this case, by a factor of about 4. Typically, I_6 becomes the dominant emission, which is reflected in its *B*-exciton and ionized donor bound *A*-exciton counterparts. This is consistent with the previously observed diffusion of Al toward the surface during annealing.[30] A noticeable difference in the visible emission is observed upon annealing. The annealed sample shows a Cu^{2+} related emission at 2.86 eV with an intense LO-phonon sideband, as first identified by Dingle.[6] This appears to be on top of another broad green emission, which is likely due to oxygen vacancies created by the vacuum annealing. Emission in the red/orange part of the spectrum is also reduced, giving the samples a strong green color when excited by the UV laser.

UV emission was observed from the Gd implanted ZnO, as shown in Fig. 3(b), but it was significantly broader and weaker than the unimplanted samples. Before annealing, the emission was reduced by more than four orders of magnitude due to the structural disorder created by the ion implantation. This disorder could be the origin of the peak near 3.37 eV in

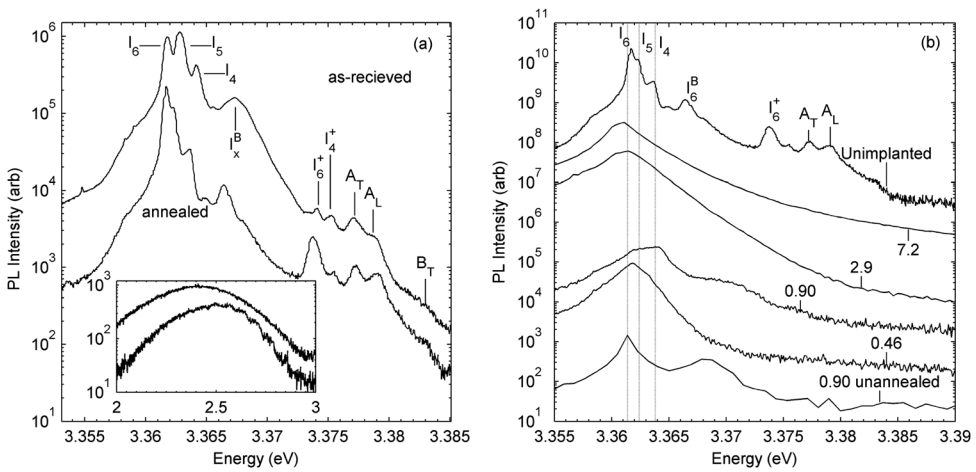

FIG. 3. (a) PL at 4 K from unimplanted ZnO before (top) and after (bottom) annealing (vertically offset for clarity). Visible emission is shown in the inset. (b) UV emission from the unimplanted and Gd-implanted ZnO after annealing (vertically offset for clarity). Implanted fluence is shown with units of 10^{15} ions cm^{-2}.

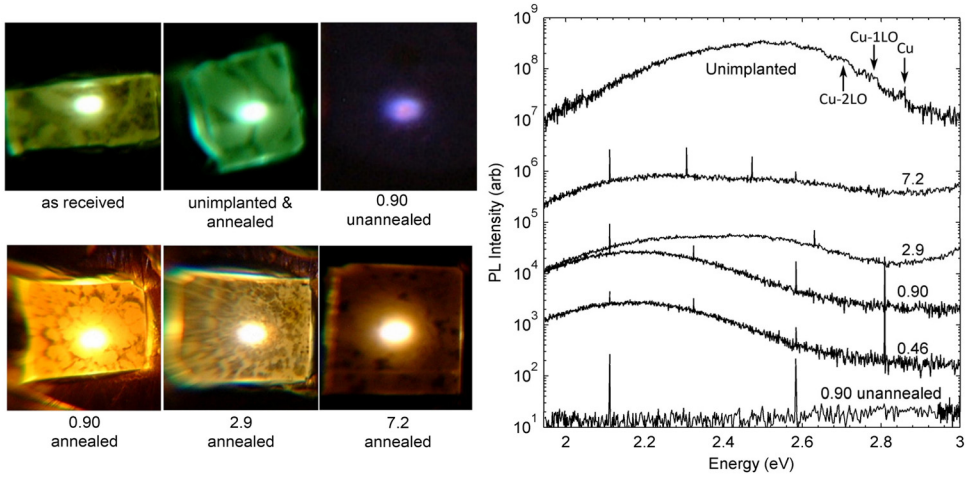

FIG. 4. (Color online) Visible PL emission at low temperature. Photographs were taken by a standard digital camera through the collecting lens. Spectra are from annealed samples and are vertically offset for clarity. The sharp lines are plasma lines from the laser which help to verify wavelength calibration. Implanted fluence is shown with units of 10^{15} ions cm^{-2}.

the 9.0×10^{14} ions cm^{-2} samples. After annealing, the implanted samples regained between 0.1 and 10% of their initial UV emission intensity. However, no signs of the free excitons were observed in any of the implanted samples. The emission seems to be dominated by the same neutral donor bound excitons as the unimplanted ZnO. At these concentrations, no transitions easily associated with Gd were observed in the UV region.

In the visible region, a notable difference was observed in the implanted samples. Figure 4 shows images and spectra of several samples. Great care must be taken in interpreting the measured spectra since the efficiency of the spectrometer has not been accounted for over the large visible range. Unfortunately, in this experiment a large amount of noise is added in some regions when applying the efficiency correction, again preventing accurate peak shape analysis. Thus, only a qualitative approach can be taken with the visible band.

Before annealing, the Gd implanted ZnO showed a very weak violet emission, with essentially no observable emission in other visible bands. This is due to the decreased PL efficiency due to the structural defects. Upon annealing, a strong orange/yellow color was observed in the implanted samples, which is significantly different than the unimplanted ZnO before and after annealing. The broad and unstructured green emission disappears, however, some Cu^{2+} emission is still observed, most notably in the 2.9×10^{15} ions cm^{-2} sample which shows a white/orange color to the eye. Passivation of the vacuum-annealing-induced oxygen vacancies is the most likely explanation for the decreased green emission. Only a small fraction of the Gd concentration used in this study would be necessary to passivate the oxygen vacancies of nearly stoichiometric ZnO, which could occur by substitution, charge exchange, complex formation, clustering, or by altering the nonradiative decay rates. However, as mentioned earlier, several other defects can also give rise to luminescence in this spectral range,[4,5,7] and they could also be passivated by the presence of the Gd. The orange/yellow color which remains is likely from a native defect, and no clear connection to Gd was observed in this study. Once the oxygen vacancy and/or other defects giving green emissions are passivated, this orange/yellow emission becomes the dominant radiative decay path.

At room temperature these samples showed a broad emission, and the spectrometer slits were opened wider to record the spectra shown in Fig. 5. Temperature dependent PL (not shown here) shows the UV emission to be composed of the free exciton recombination and its LO-phonon sidebands for all the unimplanted and Gd implanted samples. Strong visible emission was observed from all samples except those with the highest Gd concentration. This may be due to the Gd interacting with a significant fraction of the various native defects responsible for the visible emission band. Further investigation of the visible emission from these samples, or any ZnO in general, requires correlation with more data from independent sources such as electron paramagnetic resonance, thermogravimetry, or deep level transient spectroscopy.

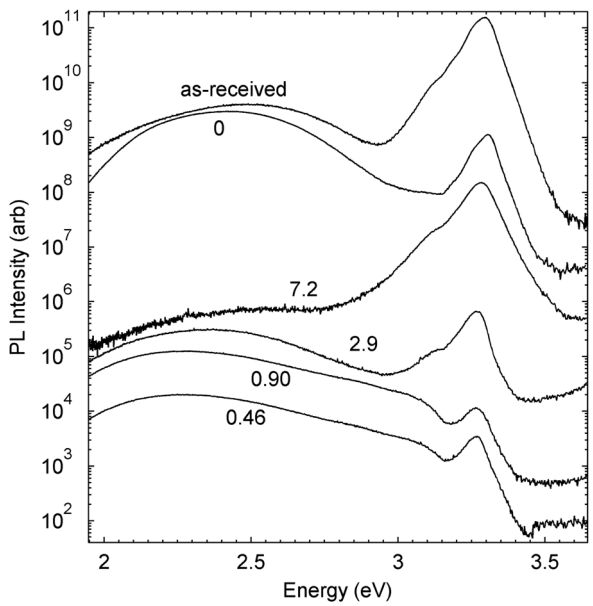

FIG. 5. Room temperature PL from the unimplanted and Gd-implanted ZnO after annealing (vertically offset for clarity). Implanted fluence is shown with units of 10^{15} ions cm^{-2}.

IV. CONCLUSIONS

The structural and photoluminescence properties have been studied for Gd implanted and annealed ZnO single crystals. The RBS/C showed that for low implantation fluences up to 85% of the Gd atoms are aligned with the ZnO [0001] crystal axis in either substitutional or shadowed sites. For higher fluences the majority of the Gd atoms are in disordered sites with likely precipitation of the Gd from the ZnO matrix. The red-shift of the A_1(LO) peak and density of phonon states-related broad peaks observed in the Raman spectra can be assigned to implantation induced defect activated features. Low temperature photoluminescence spectra suggest that the neutral donor bound exciton associated emissions are the dominant mechanism in the UV region in Gd implanted and annealed ZnO, similar to the unimplanted ZnO. Orange/yellow emission was observed in Gd implanted ZnO, in contrast to the green emission observed in unimplanted and annealed ZnO. This was most likely due to the passivation of the oxygen vacancy related green emission, which unmasked the orange/yellow emission band.

ACKNOWLEDGMENTS

The project was carried out under the research Contract No. C05X0408 from the Foundation for Research Science and Technology of New Zealand. P.P.M. acknowledges a PhD scholarship from MacDiarmid Institute for Advanced Materials and Nanotechnology.

[1]Ü. Özgür, Ya. I. Alivov, C. Liu, A. Teke, M. A. Reshchikov, S. Doğan, V. Avrutin, S.-J. Cho, and H. Morkoç, J. Appl. Phys. **98**, 041301 (2005).
[2]B. K. Meyer, H. Alves, D. M. Hofmann, W. Kriegseis, D. Forster, F. Bertram, J. Christen, A. Hoffmann, M. Straßburg, M. Dworzak, U. Haboeck, and A.V. Rodina, Phys. Status Solidi B **241**, 231 (2004).
[3]K. Vanheusden, C. H. Seager, W. L. Warren, D. R. Tallant, and J. A. Voigt, Appl. Phys. Lett. **68**, 403 (1996).
[4]M. Liu, A. H. Kitai, and P. Mascher, J. Lumin. **54**, 35 (1992).
[5]B. Lin, Z. Fu, and Y. Jia, Appl. Phys. Lett. **79**, 943 (2001).
[6]R. Dingle, Phys. Rev. Lett. **23**, 579 (1969).
[7]L. S. Vlasenko, Appl. Magn. Reson. **39**, 103 (2010).
[8]J. M. D. Coey, M. Venkatesan, and C. B. Fitzgerald, Nature Mater. **4**, 173 (2005).
[9]K. Potzger, S. Zhou, F. Eichhorn, M. Helm, W. Skorupa, A. Mücklich, J. Fassbender, T. Herrmannsdörfer, and A. Bianchi, J. Appl. Phys. **99**, 063906 (2006).
[10]V. Ney, S. Ye, T. Kammermeier, A. Ney, H. Zhou, J. Fallert, H. Kalt, F. Y. Lo, A. Melnikov, and A. D. Wieck, J. Appl. Phys. **104**, 083904 (2008).
[11]J. Qi, Y. Yang, L. Zhang, J. Chi, D. Gao, and D. Xue, Scripta Mater. **60**, 289 (2009).
[12]M. Khalid, M. Ziese, A. Setzer, P. Esquinazi, M. Lorenz, H. Hochmuth, M. Grundmann, D. Spemann, T. Butz, G. Brauer, W. Anwand, G. Fischer, W. A. Adeagbo, W. Hergert, and A. Ernst, Phys. Rev. B **80**, 035331 (2009).
[13]T. Monteiro, A. J. Neves, M. C. Carmo, M. J. Soares, M. Peres, E. Alves, E. Rita, and U. Wahl, Superlattices Microstruct. **39**, 202 (2006).
[14]Y. Q. Wang and A. J. Steckl, Appl. Phys. Lett. **82**, 502 (2003).
[15]H. J. Lozykowski, W. M. Jadwisienczak, and I. Brown, Appl. Phys. Lett. **74**, 1129 (1999).
[16]M. Peres, A. Cruz, S. Pereira, M. R. Correia, M. J. Soares, A. Neves, M. C. Carmo, T. Monteiro, A. S. Pereira, M. A. Martins, T. Trindade, E. Alves, S. S. Nobre, and R. A. Saferreira, Appl. Phys. A **88**, 129 (2007).
[17]S. W. Choi, S. Emura, S. Kimura, M. S. Kim, Y. K Zhou, N. Teraguchi, A. Suzuki, A. Yanase, and H. Asahi, J. Alloys Compds. 408-412, 717 (2006).
[18]S. Dhar, O. Brandt, M. Ramsteiner, V. F. Sapega, and K. H. Ploog, Phys. Rev. Lett. **94**, 037205 (2005).
[19]J. Kennedy, D. A. Carder, A. Markwitz, and R. J. Reeves, J. Appl. Phys. **107**, 103518 (2010).
[20]J. P. Biersack, Nucl. Instrum. Methods Phys. Res. B **27**, 21 (1987).
[21]J. R. Tesmer and M. Nastasi, Handbook for Modern Ion Beam Analysis, (Materials Research Society, Pittsburgh, 1995).
[22]R. J. Mendelsberg, J. Kennedy, S. M. Durbin, and R. J. Reeves, Curr. Appl. Phys. **8**, 283-286 (2008).
[23]J. M. Calleja and M. Cardona, Phys. Rev. B **16**, 3753 (1977).
[24]M. Schumm, M. Koerdel, S. Müller, H. Zutz, C. Ronning, J. Stehr, D. M. Hofmann, and J. Geurts, New J. Phys. **10**, 043004 (2008).
[25]Z. Q. Chen, A. Kawasuso, Y. Xu, H. Naramoto, X. L. Yuan, T. Sekiguchi, R. Suzuki, and T. Ohdaira, J. Appl. Phys. **97**, 013528 (2005).
[26]F. Friedrich and N. H. Nickel, Appl. Phys. Lett. **91**, 111903 (2007).
[27]J. Kennedy, P. Murmu, and A. Markwitz, AIP Conf. Proc. **1066**, 541 (2008).
[28]J. Serrano, A. H. Romero, F. J. Manjon, R. Lauck, M. Cardona, and A. Rubio, Phys. Rev. B **69**, 094306 (2004).
[29]N. N. Syrbu, I. M. Tiginyanu, V. V. Zalamai, V. V. Ursaki, and E. V. Rusu, Physica B **353**, 111 (2004).
[30]D. C. Look, B. Claflin, and H. E. Smith, Appl. Phys. Lett. **92**, 122108 (2008).